Letter

Puffing frequency of interacting buoyant plumes

Omkar T. Patil [1], Michael A. Meehan [2,*] and Peter E. Hamlington [2]
[1]Department of Physics, University of Colorado, Boulder, Colorado 80309, USA
[2]Paul M. Rady Department of Mechanical Engineering, University of Colorado, Boulder, Colorado 80309, USA

(Received 8 April 2022; accepted 25 October 2022; published 29 November 2022)

Buoyant plumes often pulsate, or puff, at a characteristic frequency that depends on the Richardson number. In many engineering and natural applications, however, interactions between two or more plumes can substantially affect the puffing frequency. In this study, we use numerical simulations to investigate how the plume width, W, and the separation between two plumes, S, affect the puffing frequency. The plumes are formed by injecting helium into ambient air, and we perform the simulations in two spatial dimensions to identify scaling laws in the limits of large and small S. We find that the global dependence on S closely matches that observed in reacting three-dimensional (3D) plumes, indicating that the plume dynamics are primarily connected to the presence of buoyant forces, regardless of the source of buoyancy. There is a critical value of S at which the puffing frequency changes abruptly but, in contrast to 3D reacting plumes, this critical value is independent of W for the present two-dimensional plumes. Ultimately, we find that the nonlinear decrease in puffing frequency with increasing spacing can be represented by a scaling law that depends only on S/W and the inlet Richardson number. These results allow us to identify four regimes of puffing behavior, corresponding to merged, strongly interacting, weakly interacting, and noninteracting plumes.

DOI: 10.1103/PhysRevFluids.7.L111501

I. INTRODUCTION

The puffing instability commonly observed in buoyant plumes occurs when lateral entrainment and vertical buoyancy-driven flow combine to repetitively generate vortices that rise upward against the direction of gravity. The primary method of characterizing this instability is to compute the frequency at which vortices are created, commonly referred to as the puffing frequency. This simple measurement facilitates direct comparisons between experiments, simulations, and stability analyses (see, e.g., Chakravarthy *et al.* [1], Bharadwaj and Das [2,3], and Wimer *et al.* [4]).

In the present study, we seek to understand how the puffing frequency is affected when two adjacent buoyant plumes interact. Interacting plumes occur, for example, when heat sources are in close proximity, including in buildings, electronic equipment, or when factories use smokestacks to release combustion products into the atmosphere. There are also several examples of interacting reacting plumes where buoyancy is predominantly generated as a result of heat release in the shear layer. This configuration can be found in closely spaced high temperature burners [5] or at much larger terrain scales when wildland fires interact [6]. To isolate physical mechanisms present in reacting plumes, inert buoyant plumes are often used as surrogates to capture essential flow features such as the puffing phenomenon [7,8] and bulk entrainment for unequal buoyancy sources.

*mime5507@colorado.edu

The structure and dynamics of interacting plumes are dictated by the competing effects of vortex-vortex interactions and entrainment. Buoyant plumes in an interacting pair entrain a large amount of ambient fluid [9], suggesting that vortices produced by the plumes will synchronize but remain out of phase because the entrainment varies throughout the puffing cycle. That is, when entrainment by one plume is at a maximum, entrainment by the other plume will be at a minimum, with a reversal halfway through the cycle. This behavior is in contrast to that observed in the near-field region behind bluff bodies, where vortices generated between the two adjacent shear layers have a tendency to synchronize such that they are in-phase and the vorticity in each layer is of opposite sign [10]. A low-pressure region can also form between interacting plumes (as is also seen, for example, in twin plane jets [11]), which can cause the plumes to lean toward each other and interact even more strongly [12].

Much of the prior research on interacting plumes has focused on how the interactions of multiple nonreacting sources lead to differences in downstream fluid transport. This emphasis stems from the loss of memory that occurs sufficiently far downstream from the plume source, where the flow for single plumes becomes self-similar and point-source models can be used [13]. However, the process by which finite-area sources merge for interacting plumes can significantly alter the placement of the virtual point source. Kaye and Linden [14] pioneered early theoretical work on the coalescing process in turbulent axisymmetric plumes, providing a mathematical description of the merge point and the resulting merged flow. Subsequent studies have focused on entrainment statistics [15], stratified environments [16], different plume configurations [12,17,18], and the effect of reactions [19]. Ongoing fluid transport research is generally targeted at specific applications given the wide range of inlet shapes and source types found in practice.

In the near-field of interacting plumes, by contrast, the primary focus has been on the repetitive formation of coherent vortices and the resulting puffing behavior (see, e.g., Cetegen and Ahmed [20], Wimer *et al.* [4], Hamins *et al.* [8]). Of the few researchers who have studied the frequency for interacting plumes, one clear trend has emerged. As the separation between the plumes decreases, the puffing frequency increases and the oscillations become out of phase. At a critical separation, there is a dramatic drop in the frequency and the plumes begin puffing in phase. After this point, the puffing frequency is relatively insensitive to further decreases in the separation. These observations were made as early as the 1960s [21] and have been substantiated by a number of subsequent studies [22–27]. It should be noted that, in these previous studies, the plumes were generally laminar and chemically reacting. In larger applications, such as line plumes [6], spanwise vortex breakdown may lead to interactions that are turbulent. Even though the puffing frequency has been found to scale similarly for laminar and turbulent plumes [4], it is still possible that interacting turbulent plumes will behave differently than interacting laminar plumes.

Here we build on prior research and use numerical simulations to examine how the puffing frequency depends on the separation between two identical two-dimensional (2D) helium plumes for different plume widths. The simulations use adaptive mesh refinement (AMR) to fully resolve the dynamics of interest while reducing the computational cost. We compute the puffing frequency for each simulation and seek to answer three primary questions: (i) How does the puffing frequency for 2D interacting inert plumes depend quantitatively on the plume width and separation? (ii) Are there clearly identifiable regimes of puffing behavior for different widths and separations?, and (iii) How do these results compare to previous results for 3D reacting plumes? Previous, primarily experimental, studies [22,23,28] have provided partial answers to these questions, and here we take advantage of the precision enabled by simulations to definitively answer these questions for 2D interacting plumes.

II. NUMERICAL SIMULATIONS

We perform numerical simulations of 2D interacting helium plumes using `PeleLM`, a second-order finite-volume code that solves a low-Mach formulation of the Navier-Stokes equations. A detailed discussion of the relevant transport equations and the numerical implementation is given in

Refs. [29–31]. By using helium in the simulations, the buoyancy source is not spatially evolving, by contrast to reacting flows where heat release by chemical reactions provides the primary source of buoyancy. The present focus on nonreacting plumes is motivated by Bunkwang *et al.* [28], who observed that the interactions between adjacent plumes are primarily due to flow, as opposed to chemical, effects.

The 2D computational domain in each simulation is $(4\ \mathrm{m})^2$ with a base grid of 64^2 grid cells. At $z = 0$, Dirichlet boundary conditions are used to specify the inflow. Two streams of helium with density $\rho_0 = 0.163\ \mathrm{kg/m^3}$ and viscosity $\mu_0 = 1.98 \times 10^{-5}\ \mathrm{kg/ms}$ flow into the domain through inlets of width W with velocity $V_0 = 1\ \mathrm{m/s}$ and are separated by distance S. Outside the helium streams, there is a coflow of air with density $\rho_\infty = 1.17\ \mathrm{kg/m^3}$ and viscosity $\mu_\infty = 1.86 \times 10^{-5}\ \mathrm{kg/ms}$ at velocity $V_\infty = V_0/2$. This coflow reduces numerical artifacts at the upper domain boundary, a common problem in low-speed 2D simulations [32] and also supplies ambient fluid between the two plumes. The helium inflow is transitioned to the coflow using a hyperbolic tangent profile [2]. We use a gravitational acceleration of $g = 9.81\ \mathrm{m/s^2}$ and all fluids are maintained at a temperature of $T = 300$ K. The remaining three boundary conditions are open, allowing ambient air and helium-air mixture to pass through the boundaries.

The coarse resolution of the base grid is combined with AMR to provide fine resolution near the plume source while maintaining coarse cells near the open boundaries to mitigate numerical artifacts [2,3,32]. A total of five levels of AMR are used, providing an effective grid resolution of approximately 2 mm, which was shown by Wimer *et al.* [4,29] to be sufficient for obtaining converged puffing frequencies in both laminar and turbulent plumes. To confirm the present resolution, we performed additional simulations for a subset of the cases with half and double the resolution. Comparing key metrics (e.g., puffing frequency, critical spacing), we found that the grid resolution did not impact the results presented herein. We use conservative refinement criteria based on the vorticity magnitude and cell-to-cell density differences so that the entirety of the plume is resolved to the finest level up to 0.5 m above the inlet.

The present focus on 2D simulations is motivated by physical considerations, as opposed to concerns related to the computational cost. By selecting a 2D geometry, there is a finite amount of ambient fluid between the inner shear layers. This is important because plumes entrain this fluid and, when S becomes sufficiently small, the plumes will be starved of ambient fluid between the inner shear layers, leading to a change in the puffing frequency. This is noticeably different than axisymmetric plumes where, even for $S = 0$, fluid can still be entrained near the contact point.

In the following, we examine puffing frequencies for a series of both single and double plume configurations. For the single plume case, we perform eight simulations with widths, W, varying from 5 to 12 cm while fixing all other parameter values. The single plume cases are used to validate our simulation results against prior experimental and computational studies of 2D plumes [3,33,34], as well as to provide data for comparisons with the double plume results. We perform double plume simulations for W between 5 and 12 cm and S between 0 and 14 cm; in total, 198 different double plume simulations were performed. All other parameters remain fixed for all simulations.

The resulting simulations span a range of nondimensional numbers and are designed to provide insights into the dependence of the puffing Strouhal number, $\mathrm{St} = fW/V_0$, on the width-based inlet Richardson number, $\mathrm{Ri} = (1 - \rho_0/\rho_\infty)gW/V_0^2$ and the length-scale ratio S/W, where f is the puffing frequency. The simulations span Ri from 0.42 to 1.01 and S/W between 0.018 and 2.8. Although the inlet Reynolds number, $\mathrm{Re} = \rho_0 V_0 W/\mu_0$, also varies in the simulations between 412 and 988, prior research has shown that St varies weakly with Re in buoyancy driven flows, even through the point of laminar to turbulent transition [35].

III. RESULTS AND DISCUSSION

The puffing behavior for three representative simulations is qualitatively indicated by the instantaneous snapshots of the density field shown in Fig. 1. For the single plume of width $W = 5$ cm in the top row, the vortex roll-up is regular and symmetric throughout the puffing cycle. The middle

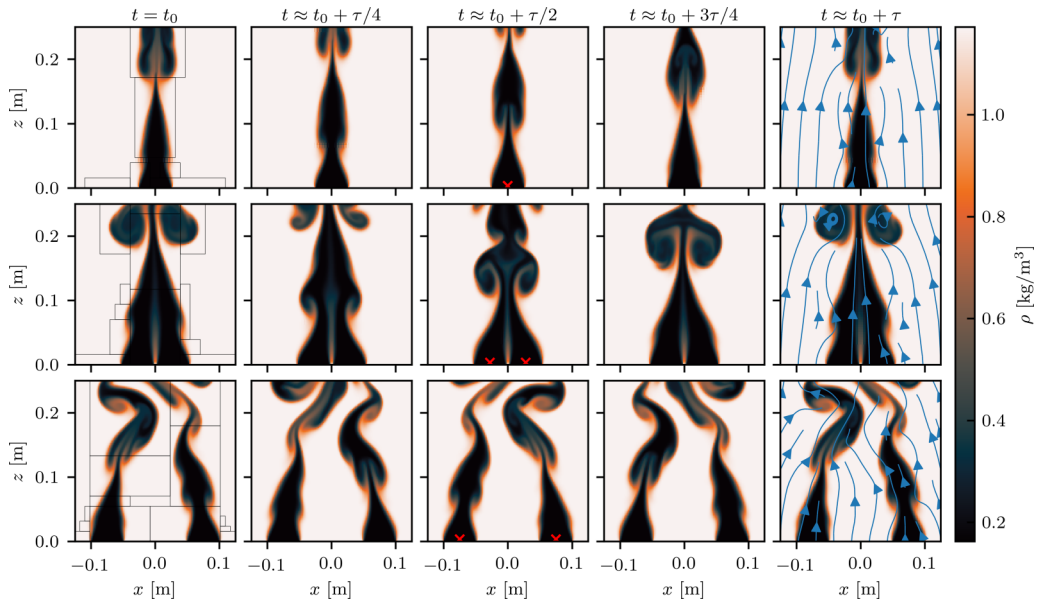

FIG. 1. Snapshots of the density field for a single plume with $W = 5$ cm (top row) and interacting plumes with $W = 5$ cm and $S = 0.6$ and 14.5 cm (middle and bottom rows, respectively). Columns from left to right show the density at time intervals of $\tau/4$, where $\tau = f^{-1}$ is the period of the puffing. The leftmost column shows where AMR is used to resolve the dynamics, the center column shows where the probes were placed in the flowfield (red arrows), and the rightmost column shows streamlines.

row in Fig. 1 shows that the puffing dynamics for small separations are quite similar to those for the single plume, except with a small density deficit near the centerline. When the separation is larger, as shown in the bottom row of Fig. 1, the flow is asymmetric about the centerline at $x = 0$, with the puffing of each plume out-of-phase. This asymmetry is most apparent by noting that the middle panel in the bottom row is almost an exact reflection about $x = 0$ compared to the leftmost and rightmost panels.

To determine the puffing frequency, f, we collected 20 s of streamwise velocity data 15 s after the start of each simulation (to allow for the decay of initial transients). Fast Fourier transforms were then applied to the time series to obtain power spectral densities (PSDs), and the peak frequency in each PSD was considered to be the puffing frequency, f. We examined time series at various spatial locations and found that the center of each plume approximately 3 mm above the inlet provided the most precise and consistent measurements of f. In general, however, f was similar across all spatial locations examined, consistent with the global nature of the associated instability [1]. The PSD for each case displays a distinct peak at a single frequency and, for the two-plume cases, the peak frequencies are the same in both left and right plumes (although, as will be shown later, the phases are not necessarily the same).

For the single plume cases, Fig. 2(a) shows f as a function of W; St is shown as a function of Ri in the inset. We then perform a linear least-squares fit and find the single-plume Strouhal number ($\mathrm{St_s}$) scaling relation

$$\mathrm{St_s} \approx c\mathrm{Ri}^{0.45}, \quad c = 0.68. \tag{1}$$

This relation closely matches previous results for single plumes [3,33,34], although the coefficient $c = 0.68$ is slightly higher than other results where $c \approx 0.5$–0.6 [3]. However, this small difference is almost certainly a consequence of the mild coflow $V_0/V_\infty = 0.5$, since Bharadwaj and Das [36] found that the presence of a coflow slightly increases the puffing frequency in axisymmetric plumes.

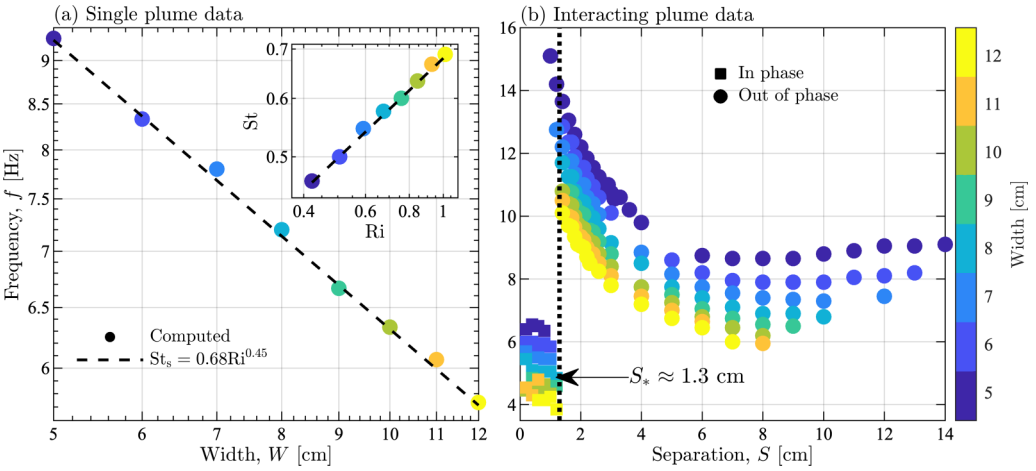

FIG. 2. Computed frequency f for (a) single plume simulations as a function of W and for (b) two-plume simulations as a function of S and W. The inset in (a) shows St as a function of Ri and the dashed lines show $\mathrm{St_s}$ from (1). Panel (b) indicates whether the two plumes puff in phase (squares) or out of phase (circles).

For the two-plume cases, Fig. 2(b) shows that f increases for all S with decreasing W and is independent of S for sufficiently small and large separations. Figure 2(b) also effectively summarizes the values of W and S used in each of the 198 two-plume simulations performed here. For intermediate values of S, f increases with decreasing S until a *critical separation*, denoted S_*, is reached and there is an abrupt drop in f. The phase difference between the two plumes is also indicated in Fig. 2(b), where the puffing goes from in phase to out of phase with increasing S at S_*. To compute the phase difference, we found the angles of the complex value associated with the peak frequencies in the PSDs. Using symmetry, the magnitude of the difference between the angles of the different plumes is then the phase difference between the plumes, which we denote ϕ. When $\phi \approx \pi$, the plumes are out of phase, and when $\phi \approx 0$, the plumes are in phase. For the simulations presented here, $\phi \approx 0$ or $\phi \approx \pi$ in all cases, allowing us to unambiguously define in-phase and out-of-phase puffing between the plumes.

We quantitatively determine S_* for each W by iterating through the cases from large S and identifying the first value of S where the plumes change from out of phase to in phase; S_* must then lie between this and the previous value of S. The average of these separations is remarkably consistent for different W, with $S_* \approx 1.3 \pm 0.1$ cm for all but the smallest W, where $S_* \approx 0.9 \pm 0.1$ cm. The error is approximated from the difference in separations used to calculate the average. Although a similar decrease in puffing frequency was observed for decreasing S in reacting plumes, the present independence of S_* on W is in contrast to reacting axisymmetric (i.e., 3D) plumes where the critical spacing increases with the diameter of the plume, D, as $S_* \sim D^{1/3}$ [28].

Previously, the abrupt frequency change at S_* has been hypothesized to depend on radiation [22], vortex dynamics [37], and viscosity [24,28]. In the present study, the consistency of S_* across all cases suggests that the critical separation may depend on other parameters not varied here, for example the viscosity and the buoyancy length scale V_0^2/g. Determining how S_* depends on these and other parameters would require many additional simulations, but this is nevertheless the most important future research direction suggested by the present study.

To determine a relation for St in the two-plume case, Fig. 3(a) shows $\mathrm{St}/\mathrm{St_s}$ as a function of S/W for different Ri (note that Ri is a direct nondimensional surrogate for W in the present study, since W is the only parameter in Ri that varies in the simulations). With this normalization, Fig. 3(a) shows that the plumes approach the spacing-independent single plume value $\mathrm{St}/\mathrm{St_s} \approx 1$ for $S/W \gg 1$, corresponding to the limit where the two plumes become decoupled and puff independently. We correspondingly call $S/W \gg 1$ the *noninteracting* regime and $S/W \gtrsim 1$ the *weakly interacting*

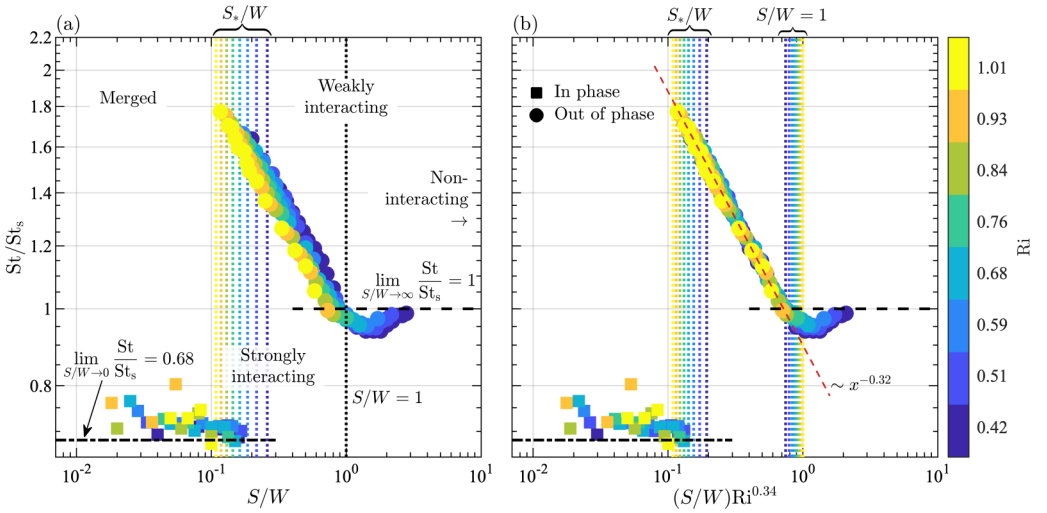

FIG. 3. Two-plume puffing Strouhal number St normalized by St_s from (1) as a function of (a) S/W and (b) $(S/W)Ri^{0.34}$. Panel (b) shows the empirically determined scaling relation in the strongly interacting regime, summarized in (2). In both panels, squares indicate in-phase puffing and circles indicate out-of-phase puffing.

regime. Within the weakly interacting regime, St is slightly below the single plume value, although we do find that $St/St_s \approx 1$ by $S/W \approx 3$ for all Ri.

The plume oscillations in the weakly interacting regime are out of phase due to variations in the amount of mass entrained by each plume during the puffing cycle, ultimately causing the two plumes to entrain mass maximally (or minimally) at different times. Although the present simulations do not extend far into the noninteracting regime, there is no reason for any phase relationship to exist between the plumes in this regime, beyond the numerical coupling imposed by the finite size of the computational domain in the simulations.

For $S/W \lesssim S_*/W$, the two plumes puff in phase and eventually merge as $S/W \to 0$, resulting in a puffing frequency that corresponds to a single plume of width $2W$, giving $St/St_s = 2^{1-0.45} = 0.68$. In this *merged* regime, Fig. 3(a) shows that the computed frequencies are all slightly above $St/St_s = 0.68$, most likely due to the nonzero coflow velocity. However, the statistical variability of the data in the merged regime is too large to draw any quantitative conclusions regarding the scaling of St/St_s for small S/W. For intermediate values of S/W where $S/W \geqslant S_*/W$ and $S/W \lesssim 1$, the plumes are close and Fig. 3(a) shows that there is a self-induced increase in St/St_s with decreasing S/W. This is the *strongly interacting* regime which begins (with decreasing S/W) at the *transitional separation* $S/W \approx 1$. This is a common transitional scale in other interacting flows, such as interacting bluff bodies [38,39].

Although St/St_s nearly collapses for all Ri in the strongly interacting regime, Fig. 3(a) shows that there is still a residual dependence on Ri. This additional dependence on Ri is accounted for in Fig. 3(b), where St/St_s is shown as a function of $(S/W)Ri^{0.34}$. The exponent 0.34 was empirically determined using a linear regression to give the best collapse of the data in the strongly interacting regime, and an additional least-squares fit shows that $St/St_s = 0.9[(S/W)Ri^{0.34}]^{-0.32}$ provides an accurate scaling relation in this regime. For the interacting double plume configuration we can thus summarize the dependence of St on S/W and Ri as

$$St \approx \begin{cases} 0.46Ri^{0.45} & \text{for} \quad 0 \leqslant S/W < S_*/W \\ 0.61(S/W)^{-0.32}Ri^{0.34} & \text{for} \quad S_*/W \leqslant S/W \lesssim 1, \\ 0.68Ri^{0.45} & \text{for} \quad S/W \gg 1 \end{cases} \tag{2}$$

where $S_* = 1.3$ cm is the critical separation for the present simulations.

IV. CONCLUSIONS

Using numerical simulations, we have examined the effects of the plume width, W, and separation, S, on the puffing frequency of 2D interacting helium plumes. Consistent with results for axisymmetric interacting plumes with reactions, we find that, as S decreases, the frequency increases nonlinearly until a critical separation, denoted S_*, at which the frequency decreases abruptly. By contrast to 3D reacting plumes, however, we find that S_* is independent of W in the present 2D plumes. For small S/W corresponding to the merged regime, the puffing Strouhal number, St, is independent of S/W and consistent with results for a single plume with width $2W$. Within the strongly interacting regime for $S_*/W \leqslant S/W \lesssim 1$, St increases with decreasing S/W and increasing Richardson number, Ri. In the weakly interacting regime for $S/W \gtrsim 1$, St is slightly below the single plume value found in the noninteracting regime. For $S/W \gg 1$, corresponding to the noninteracting regime, St approaches results for a single plume of width W. The plume oscillations are in phase in the merged regime, out of phase in the strongly and weakly interacting regimes, and should become fully decoupled in the noninteracting regime, as shown by Dange *et al.* [23].

With these conclusions, we have addressed the three questions outlined in the introduction. However, this study also introduces several new research directions. First, it may be possible to analytically derive the scaling relationship in the strongly interacting regime, where the exponents on both S/W and Ri in (2) are close to $1/3$. Second, additional simulations exploring different parameters, particularly with differences between sources [14], would enable (2) to be generalized even further, including a better estimate of S_* based on inlet parameters. Finally, extending these results to turbulent 3D line plumes is important for many practical applications.

ACKNOWLEDGMENTS

O.T.P. was supported, in part, by the Discovery Learning Apprentice Program at the University of Colorado, Boulder. M.A.M. was supported by the NSF Graduate Research Fellowship Program Award No. 2018262982. M.A.M. and P.E.H. were supported, in part, by AFOSR Award No. FA9550-18-1-0057 and NSF Award No. 1847111. This work used the Frontera supercomputer at the Texas Advanced Computing Center (TACC) at the University of Texas at Austin.

[1] R. Chakravarthy, L. Lesshafft, and P. Huerre, Global stability of buoyant jets and plumes, J. Fluid Mech. **835**, 654 (2018).

[2] K. K. Bharadwaj and D. Das, Global instability analysis and experiments on buoyant plumes, J. Fluid Mech. **832**, 97 (2017).

[3] K. K. Bharadwaj and D. Das, Puffing in planar buoyant plumes: BiGlobal instability analysis and experiments, J. Fluid Mech. **863**, 817 (2019).

[4] N. Wimer, C. Lapointe, J. Christopher, S. Nigam, T. Hayden, A. Upadhye, M. Strobel, G. Rieker, and P. Hamlington, Scaling of the puffing Strouhal number for buoyant jets and plumes, J. Fluid Mech. **895**, A26 (2020).

[5] C. E. Baukal, *Heat Transfer in Industrial Combustion* (CRC Press Boca Raton, FL, 2000), Vol. 568.

[6] M. A. Finney and S. S. McAllister, A review of fire interactions and mass fires, J. Combust. **2011**, 1 (2011).

[7] A. F. Ghoniem, I. Lakkis, and M. Soteriou, Numerical simulation of the dynamics of large fire plumes and the phenomenon of puffing, in *Symposium (International) on Combustion* (Elsevier, Naples, Italy, 1996), Vol. 26, pp. 1531–1539.

[8] A. Hamins, J. Yang, and T. Kashiwagi, An experimental investigation of the pulsation frequency of flames, in *Symposium (International) on Combustion* (Elsevier, Sydney, Australia, 1992), Vol. 24, pp. 1695–1702.

[9] X. Jiang and K. Luo, Spatial direct numerical simulation of the large vortical structures in forced plumes, Flow, Turbul. Combust. **64**, 43 (2000).
[10] A. Prasad and C. H. Williamson, The instability of the shear layer separating from a bluff body, J. Fluid Mech. **333**, 375 (1997).
[11] E. Tanaka, The interference of two-dimensional parallel jets: 2nd report, experiments on the combined flow of dual jet, Bull, JSME **17**, 920 (1974).
[12] A. C. Lai and J. H. Lee, Dynamic interaction of multiple buoyant jets, J. Fluid Mech. **708**, 539 (2012).
[13] F. J. Diez and W. J. Dahm, Effects of heat release on turbulent shear flows. Part 3. Buoyancy effects due to heat release in jets and plumes, J. Fluid Mech. **575**, 221 (2007).
[14] N. Kaye and P. Linden, Coalescing axisymmetric turbulent plumes, J. Fluid Mech. **502**, 41 (1999).
[15] C. Cenedese and P. Linden, Entrainment in two coalescing axisymmetric turbulent plumes, J. Fluid Mech. **752**, R2 (2014).
[16] Y. Lou, Z. He, H. Jiang, and X. Han, Numerical simulation of two coalescing turbulent forced plumes in linearly stratified fluids, Phys. Fluids **31**, 037111 (2019).
[17] G. Rooney, Merging of a row of plumes or jets with an application to plume rise in a channel, J. Fluid Mech. **771**, R1 (2015).
[18] G. Rooney, Merging of two or more plumes arranged around a circle, J. Fluid Mech. **796**, 712 (2016).
[19] T. Maynard, M. Princevac, and D. R. Weise, A study of the flow field surrounding interacting line fires, J. Combust. **2016**, 1 (2016).
[20] B. M. Cetegen and T. A. Ahmed, Experiments on the periodic instability of buoyant plumes and pool fires, Combust. Flame **93**, 157 (1993).
[21] T. Y. Toong, Mechanisms of combustioninstability, in *Symposium (International) on Combustion* (Elsevier, Cambridge, England, 1965), Vol. 10, pp. 1301–1313.
[22] H. Kitahata, J. Taguchi, M. Nagayama, T. Sakurai, Y. Ikura, A. Osa, Y. Sumino, M. Tanaka, E. Yokoyama, and H. Miike, Oscillation and synchronization in the combustion of candles, J. Phys. Chem. A **113**, 8164 (2009).
[23] S. Dange, S. A. Pawar, K. Manoj, and R. Sujith, Role of buoyancy-driven vortices in inducing different modes of coupled behaviour in candle-flame oscillators, AIP Adv. **9**, 015119 (2019).
[24] T. Yang, X. Xia, and P. Zhang, Vortex-dynamical interpretation of anti-phase and in-phase flickering of dual buoyant diffusion flames, Phys. Rev. Fluids **4**, 053202 (2019).
[25] L. Changchun, L. Xinlei, G. Hong, D. Jun, Z. Shasha, W. Xueyao, and C. Fangming, On the influence of distance between two jets on flickering diffusion flames, Combust. Flame **201**, 23 (2019).
[26] N. Fujisawa, K. Imaizumi, and T. Yamagata, Synchronization of dual diffusion flame in co-flow, Exp. Thermal Fluid Sci. **110**, 109924 (2020).
[27] A. Bunkwang, T. Matsuoka, and Y. Nakamura, Similarity of dynamic behavior of buoyant single and twin jet-flame(s), J. Therm. Sci. Technol. **15**, JTST0028 (2020).
[28] A. Bunkwang, T. Matsuoka, and Y. Nakamura, Mode transition of interacting buoyant non-premixed flames, J. Therm. Sci. Technol. **15**, JTST0003 (2020).
[29] N. T. Wimer, M. S. Day, C. Lapointe, M. A. Meehan, A. S. Makowiecki, J. F. Glusman, J. W. Daily, G. B. Rieker, and P. E. Hamlington, Numerical simulations of buoyancy-driven flows using adaptive mesh refinement: Structure and dynamics of a large-scale helium plume, Theor. Comput. Fluid Dyn. **35**, 61 (2021).
[30] M. S. Day and J. B. Bell, Numerical simulation of laminar reacting flows with complex chemistry, Combust. Theory Model. **4**, 535 (2000).
[31] A. Nonaka, M. S. Day, and J. B. Bell, A conservative, thermodynamically consistent numerical approach for low Mach number combustion. Part I: single-level integration, Combust. Theor. Model. **22**, 156 (2018).
[32] J. Craske and M. van Reeuwijk, Robust and accurate open boundary conditions for incompressible turbulent jets and plumes, Comput. Fluids **86**, 284 (2013).
[33] B. Cetegen, Y. Dong, and M. Soteriou, Experiments on stability and oscillatory behavior of planar buoyant plumes, Phys. Fluids **10**, 1658 (1998).

[34] M. Soteriou, Y. Dong, and B. Cetegen, Lagrangian simulation of the unsteady near field dynamics of planar buoyant plumes, Phys. Fluids **14**, 3118 (2002).
[35] M. A. Meehan, T. W. Nicholas, and E. H. Peter, Richardson and Reynolds number effects on the near field of buoyant plumes: temporal variability and puffing, J. Fluid Mech. **950**, A24 (2022).
[36] K. K. Bharadwaj and D. Das, Influence of coflow on buoyant plume puffing, J. Fluids Eng. **143**, 091303 (2021).
[37] K. Okamoto, A. Kijima, Y. Umeno, and H. Shima, Synchronization in flickering of three-coupled candle flames, Sci. Rep. **6**, 1 (2016).
[38] D. Sumner, Two circular cylinders in cross-flow: A review, J. Fluids Struct. **26**, 849 (2010).
[39] M. Meehan, A. Tyagi, and J. OConnor, Flow dynamics in a variable-spacing, three bluff-body flowfield, Phys. Fluids **30**, 025105 (2018).